Effects on Electronic Properties of Molecule Adsorption on CuO Surfaces and Nanowires†

Jun Hu,‡ Dongdong Li,§,|| Jia G. Lu,§ and Ruqian Wu*,‡

Department of Physics and Astronomy, University of California, Irvine, California 92697-4575, Department of Physics and Astronomy and Department of Electrical Engineering, University of Southern California, Los Angeles, California 90089-0484, and School of Materials Science and Engineering, Shanghai Jiao Tong University, Shanghai 200240, China

Received: April 29, 2010; Revised Manuscript Received: July 6, 2010

First-principles calculations were performed to study the stabilities, electronic structures, and chemical activities of various CuO surfaces for the understanding of the gas-induced change of conductance of CuO nanowires. It was found that CuO(111) and CuO($\bar{1}$11) have the lowest surface energies under ambient conditions and hence should be the most preferential facets of CuO nanowires. While band gaps of these surfaces are narrower than that of bulk CuO, they maintain the semiconductor feature. Adsorption of oxidizing gas such as O_2 or NO_2 on the CuO(111) and CuO($\bar{1}$11) surfaces induces metallic behavior, and molecules gain electrons from the substrates. These two effects result in an increase of hole density and hence enhance the surface conductivity of CuO nanowires as observed in our experiments. On the contrary, adsorption of H_2O molecules on CuO(111) not only widens the band gap but also donates electrons to the surface, which leads to reduction of surface conductivity. In addition, we found that CuO(111) is potentially an efficient catalyst for CO oxidation through the Mars−van Krevelen mechanism.

I. Introduction

Metal oxide semiconductor nanowires (MOSNWs) have attracted extensive attention due to their extraordinary physical properties that are usable for applications such as gas sensor, nanoelectronics, and nanocatalysis.[1–4] Cupric oxide (monoclinic CuO) is of particular interest since it is one of the few intrinsic *p-type* semiconductors with a narrow band gap (1.2−1.9 eV)[5–8] and hence it can be used for fabrication of p−n heterojunctions with other *n-type* metal oxides such as ZnO and TiO_2.[9] CuO and Cu_2O surfaces were also found to have excellent catalytic activity and selectivity toward oxidation of propylene and may convert hydrocarbons completely into carbon dioxide and water.[10] Furthermore, CuO may find applications in lithium-ion batteries and field emission devices. Recent success of fabricating CuO nanowires (NWs) adds another dimension for the control of physical and chemical properties of CuO, via the strong size dependent quantum confinement effect. To develop efficient gas sensors, several groups have studied the sensitivity of conductance of CuO NWs to C_2H_5OH, H_2S, H_2, CO, NH_3, and NO_2 molecules.[11–14] However, this effort has been somewhat hindered since experimental results are rather controversial and the mechanism behind the change of conductance of NWs is still very vague.[15] For utilization of CuO nanostructures in different technologies, it is crucial to attain clear fundamental understanding of their physical properties, starting from studies of their stable geometries and interaction with simple gas molecules.

Compared to extensive explorations for the n-type MOSNWs, studies for CuO are inadequate. Fundamentally, cupric oxide is a Mott insulator and is believed to share lots of common ground in physics with high-T_C superconductors and spintronics oxides.[16] Bulk CuO has an antiferromagnetic (AFM) ground state, with a Néel temperature in the 213−230 K range. It is intriguing that CuO NWs may show ferromagnetic behavior from 5 K to room temperature,[17] due to the large surface/bulk ratio and also the uncompensated exchange interaction with neighbors in the surface region. In general, a CuO NW consists of several facets, and those with the largest surface areas should play the most important role to gas sensing, magnetization, and catalysis. While transmission electron microscope (TEM) images and X-ray diffractions show that CuO NWs form ordered crystalline structures, it is nevertheless unclear regarding the shape of their cross sections and the orientations of their most preferential facet(s). This might be the most critical bottleneck for the further understanding of surface behaviors of CuO NWs toward foreign adsorbates. For typical CuO NWs that are 30−100 nm in diameter, their optimal shape of cross section can be determined according to the Wulff plot, using surface energies calculated from density functional simulations. Their catalytic activity and sensitivity can also be understood through studies of adsorption problems on several preferential surfaces.

Here we report results of systematic theoretical investigations for surface energies of various low-index CuO surfaces. We found that CuO(111) and CuO($\bar{1}$11) are much more stable than other surfaces and thus assigned them as the most important facets of CuO nanowires. We further studied adsorptions of O_2, NO_2, H_2O, C_2H_5OH, and CH_3CHO molecules on CuO surfaces to explain our recent experimental findings[18] of the unusual sensitivity of CuO NWs to these gases. Significant charge transfer between the CuO substrate and adsorbates was found to be the chief reason for the change of conductivity of CuO NWs upon the exposure to different gas environments.

II. Method and Computational Details

All calculations were carried out with the Vienna ab initio simulation package (VASP),[19] at the level of the generalized-gradient approximation (GGA).[20] We used the projector aug-

† Part of the "D. Wayne Goodman Festschrift".

* Author to whom the correspondence should be addressed, wur@uci.edu.
‡ University of California, Irvine.
§ University of Southern California.
|| Shanghai Jiao Tong University.

10.1021/jp1039089
Published on Web 07/22/2010

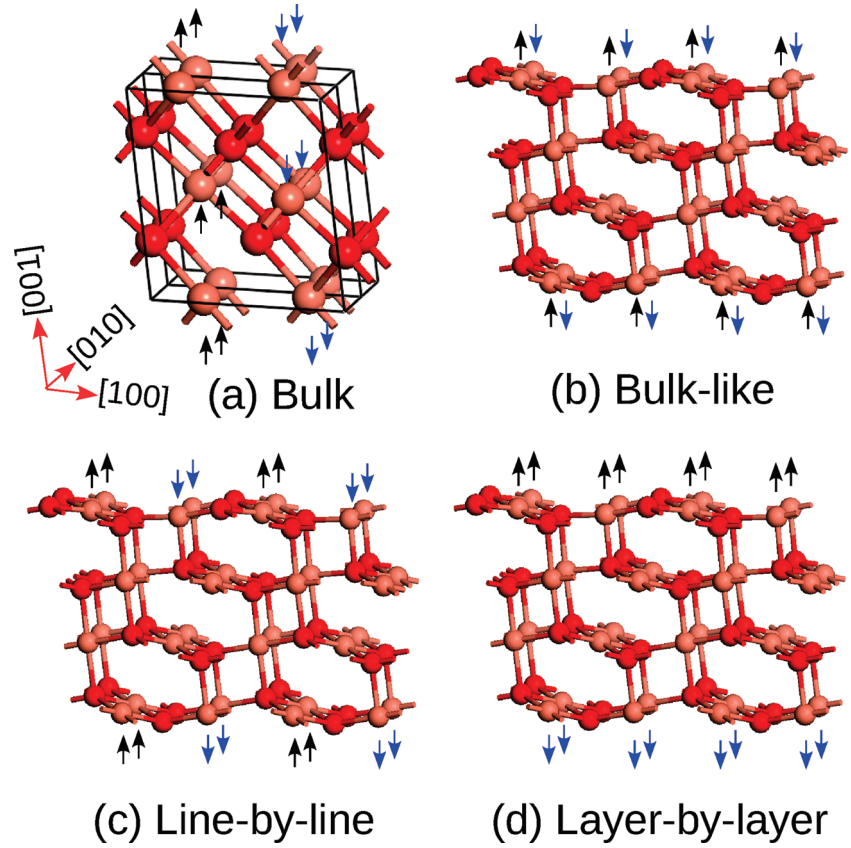

Figure 1. (a) Ground-state magnetic ordering of the bulk CuO. (b−d) Three possible magnetic orderings of CuO(111). Arrows are given for the surface atoms only for the purpose of clarity. The salmon pink and red balls represent Cu and O atoms, respectively.

mented wave (PAW) method for the description of core−valence interaction.[21] Since the bulk CuO has an antiferromagnetic ground state, spin polarization was considered for all cases. The energy cutoff of plane wave expansion was set to 400 eV. For the bulk CuO, an 11 × 11 × 11 *k*-grid mesh within the Monkhorst−Pack scheme[22] in the Brillouin zone was employed. For CuO surfaces, we used a 2 × 2 supercell in the lateral plane and the two-dimensional Brillouin zone was sampled with a 7 × 7 *k*-grid mesh. All CuO slabs are thicker than than 12 Å, with a 15−18 Å vacuum in between. The atomic positions were fully relaxed using the conjugated gradient method for energy minimization until calculated force on each atom is smaller than 0.01 eV/Å.

It is known that the strong correlation effect among Cu 3d electrons in CuO is crucial for the correct description of its ground state properties. CuO is intrinsically a p-type semiconductor with a band gap of 1.2−1.9 eV.[5−8] However, we found that conventional GGA calculations produced a metallic ground state, a result which is obviously wrong. This can be fixed by introducing the Hubbard *U* correction,[23−25] through the GGA + U method formulated by Dudarev et al.[26] In this work, parameters (*U* and *J*) were adopted from ref 23, namely, *U* = 7.5 eV and *J* = 0.98 eV. As a result, we obtained an antiferromagnetic ground state, with a local magnetic moment of 0.63 μ_B per Cu atom, in excellent agreement with previous calculations[25] and experimental measurements.[27,28] In this state, spin moments of Cu atoms are parallel to each other within the (100) planes, as depicted in Figure 1a. A band gap (E_g) of 1.1 eV was obtained, as shown in the curves of density of states in Figure 2a. Clearly, the GGA + U approach and the *U* and *J* parameters are appropriate for the description of the CuO bulk. Since Cu 3d orbitals are rather localized, we adopted the same values of *U* and *J* for surface calculations.

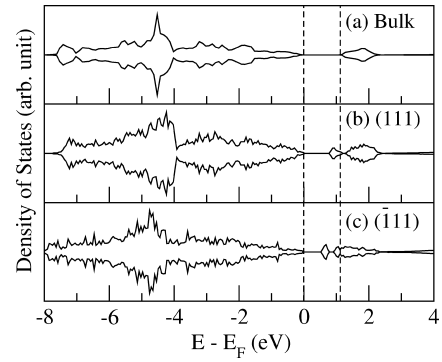

Figure 2. Density of states of (a) bulk CuO, (b) CuO(111), and (c) CuO($\bar{1}$11). The vertical dashed lines highlight the range of band gap of bulk CuO.

To investigate the stability of various low index CuO surfaces, we define their surface free energies at temperature *T* and pressure *p* as[29]

$$\gamma(T,p) = \frac{1}{2A}[G(T,p,N_{Cu},N_O) - N_{Cu}\mu_{Cu}(T,p) - N_O\mu_O(T,p)] \quad (1)$$

Here *A* is the surface area; $G(T, p, N_{Cu}, N_O)$ is the Gibbs free energy of the slab; N_{Cu} and N_O are the numbers of Cu and O atoms; μ_{Cu} and μ_O are the chemical potentials for Cu and O with a constraint: $\mu_{Cu} + \mu_O = \mu_{CuO}$. Under ambient conditions, the effects of *T* and *p* on the Gibbs free energy are negligible. Therefore, $\gamma(T, p)$ can be approximately replaced by the total energy difference from the first-principles calculations. In the following, we neglect the influence of *T* and *p* and use γ for $\gamma(T, p)$.

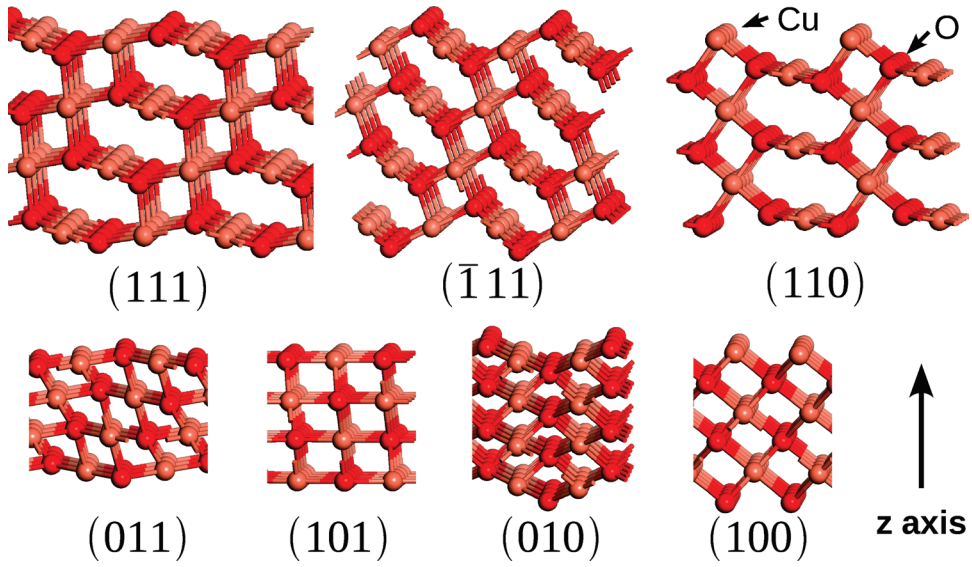

Figure 3. Structure models of CuO surfaces considered in this work. For clarity, the thicknesses of slabs are much smaller than those used in calculations.

TABLE 1: Surface Free Energies (γ, in unit of J/m^2) and Work Functions (Φ, in units of eV) of Stoichiometric CuO Surfaces

	(111)	(1̄11)	(011)	(101)	(110)	(010)	(100)
γ	0.74	0.86	0.93	1.16	1.29	1.37	2.28
Φ	5.8	5.8	5.6	5.3	6.3	5.6	7.6

III. Results and Discussion

A. CuO Surfaces. Seven different low-index surfaces were studied, with their structures given in Figure 3. Most slab models we used have two identical surfaces, except the CuO(110) and CuO(100) slabs. To construct symmetric models for these two slabs, one can either remove the topmost Cu layer or attach an additional Cu layer to the bottom surface. This modification leads to nonstoichiometric slab models with either O- or Cu-terminated surfaces on both sides.

The values of γ of the stoichiometric models in Table 1 indicate that CuO(111) is the most stable surface, with a γ of 0.74 J/m^2. CuO(1̄11) is slightly higher in energy, with a γ of 0.86 J/m^2. In the opposite side, γ of CuO(100) is 2.28 J/m^2, much larger than those of others, mainly because of the existence of a high electrostatic field between the cationic and anionic surfaces. For the same reason, the surface energy of the stoichiometric CuO(110) is also high, 1.29 J/m^2. However, as a common phenomenon in oxides,[30] it is known that their surface energies can be significantly modified by oxygen pressure, especially for nonstoichiometric surfaces. To quantify this effect, we also calculated surface energies of the O- and Cu-terminated CuO(110) and CuO(100) slabs. The values of γ of O-terminated CuO(110) [CuO(110)$_O$] and Cu-terminanted CuO(110) [CuO(110)$_{Cu}$] are plotted in Figure 4 as a function of the O chemical potential. In the O-rich regime, CuO(110)$_O$ is more stable than CuO(110)$_{Cu}$ and stoichiometric CuO(110). As the oxygen pressure decreases, or equivalently μ_O increases, the surface energy of CuO(110)$_O$ goes up, whereas that of CuO(110)$_{Cu}$ drops. Overall, the stoichiometric CuO(110) surface can hardly exist within the entire range of μ_O. It should be noted that CuO(110)$_O$ is even more stable than CuO(111), in a narrow range near the limit of O-rich condition ($\mu_O \sim -1.6$ eV). However, this relatively extreme condition is not easily achievable in typical experiments. Similarly, for the CuO(100) surface, CuO(100)$_O$, and CuO(100)$_{Cu}$ are relatively more stable in the O-rich and O-poor conditions, respectively. Although the best value of γ of CuO(100) is substantially reduced to 1.51 J/m^2 from that of the stoichiometric slab, it is still much higher than that of CuO(111). Therefore, we believe that CuO(111) is the most probable facet of a CuO NW, possibly along with CuO(1̄11). We found that the work functions of CuO(111) and CuO(1̄11) are 5.8 eV, as listed in Table 1. This value agrees well with experimental data, 5.3 eV,[7] suggesting the reliability of our atomic models for the simulation of actual CuO surfaces and NWs.

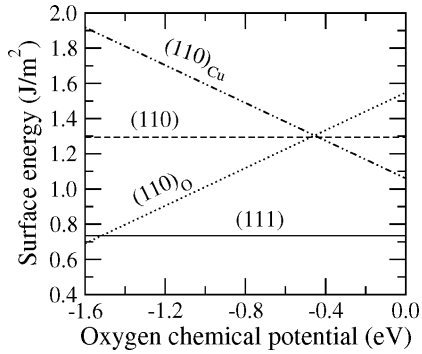

Figure 4. Surface energies of CuO(110) with different termination as a function of oxygen chemical potential. Values of -1.6 and 0.0 eV correspond the limits of O-rich and O-poor conditions, respectively.

Because the z-symmetry is broken, magnetic properties of CuO surfaces should be notably altered. It is hence important to figure out the best magnetic configurations for different CuO surfaces. Since we ruled out the presence of many CuO surfaces in CuO NWs based on their surface energies, we concentrate on the results of CuO(111) and CuO(1̄11) below. For each of them, we considered three different magnetic configurations: layer-by-layer, line-by-line, and bulklike orderings, as depicted in Figure 1. From total energies, we found that CuO(111) prefers the bulklike spin ordering. The layer-by-layer and line-by-line spin orderings increase γ by 0.21 and 0.02 J/m^2, respectively. On the other hand, CuO(1̄11) adopts the layer-by-layer spin ordering with an even number of layers. However, the energy differences among these three configurations are less than 0.05 J/m^2. Slight changes of magnetic moments were also found with respect to the bulk CuO. For CuO(111), while magnetic

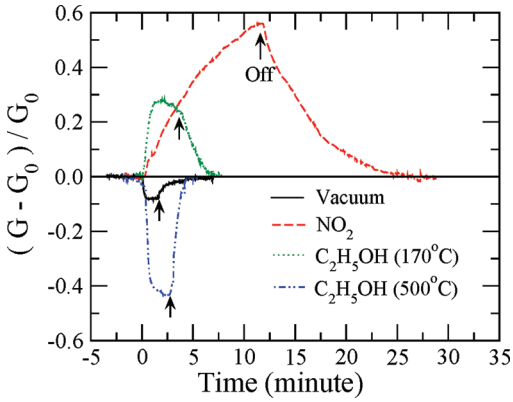

Figure 5. The change of conductance of a CuO NW exposed to different environments. G_0 and G stand for the conductances before and after exposure to gas molecules. Gases are switched on at zero time, and the arrows indicate the time when gases are switched off.

moments of all four-coordinate Cu atoms retain the bulk value, 0.63 μ_B, three-coordinate Cu atoms in the surface layer have 0.57 μ_B. Interestingly, about 0.10 μ_B magnetic moments are induced in the three-coordinate O surface atoms, since their p_z orbitals are not fully occupied with Cu−O bonds missing along the z axis (see Figure 3). The magnetic moments of these O atoms are antiparallel to each other, so they do not contribute to the net magnetic moment of the whole system. For CuO($\bar{1}$11), magnetic moments of the four- and three-coordinate Cu atoms are 0.62 and 0.53 μ_B, respectively. Similar to CuO(111), the three-coordinate O surface atoms possess local magnetic moments of about 0.15 μ_B, but they also cancel each other due to the antiparallel alignment. The density of state (DOS) values of CuO(111) and CuO($\bar{1}$11) are plotted in Figure 2. It is clear that these surfaces keep the bulklike semiconducting behavior, but their E_g values are reduced to 0.79 eV for CuO(111) and 0.55 eV for CuO($\bar{1}$11). Since peaks of surface states sit right in the bulk band gap, we expect that they do not penetrate deeply into the bulk region.

B. Adsorption of Gas Molecules and the Effect on Carrier Density. Now we turn our attention to adsorption of gas molecules on CuO surfaces, mainly CuO(111), so as to address the mechanism of our recent experimental findings regarding the gas-induced change of conductance of CuO NWs.[18] These studies are also of broad interests for the understanding of adsorption and catalysis on oxide surfaces. Here we briefly summarize the most critical experimental results and leave the detailed description for the experimental procedures for a publication elsewhere.[18] As shown in Figure 5, taking the conductance of a CuO NW in air as the reference, environments can be sorted into two categories: (i) NO_2 and C_2H_5OH (at 170 °C) that enhance the conductance; (ii) vacuum and C_2H_5OH (at 500 °C) that reduce the conductance. It can also be seen that CuO NWs respond to all circumstances rather quickly except to NO_2 gas. To disclose the mechanism behind these findings, we investigated the adsorption of various gas molecules on CuO surfaces.

We first discuss the reference system: adsorption of O_2 molecules on CuO(111). In air, CuO NWs should be covered with O_2 molecules, as evidenced by the drop of conductance when the air pressure is gradually reduced to vacuum. As in Figure 3, the most probable sites for O_2 adsorption on CuO(111) are above the unsaturated three-coordinate Cu and O atoms. For the convenience of discussions, we denote these atoms as Cu_{us} and O_{us} below. After optimizing several initial geometries for O_2/CuO(111), including the side-on mode with two oxygen atoms interacting with separate Cu_{us} atoms, we found that O_2 prefers to bind to the Cu_{us} site as depicted in Figure 6a. This can be easily understood, since O_2 tends to oxidize the unsatured Cu_{us} ions. The shortest O−Cu_{us} bond length in O_2/CuO(111) is 2.03 Å, which is only slightly longer than that between Cu and O ions in the bulk CuO. Nonetheless, the attraction between O_2 and CuO(111) is actually weak since the binding energy (E_b) is only 0.27 eV per O_2 molecule.

To understand the effect of O_2 on the transport property of CuO NWs, the DOS of O_2/CuO(111) is displayed in Figure 7b. Interestingly, adsorption of O_2 on CuO(111) surface induces states at the Fermi level. This O_2 induced metallic feature appears to be the reason why the conductance of CuO NWs decreases when O_2 coverage is reduced in vacuum. However, one needs to be cautious to view this feature, due to the fact that E_b of O_2/CuO(111) is very low. According to the Langmuir equation, the covering ratio of gas molecules (θ) at temperature T and pressure p can be expressed as

$$\theta = \frac{p}{p + p_0(T)} \tag{2}$$

with

$$p_0(T) = \left(\frac{2\pi mkT}{h^2}\right)^{3/2} e^{-E_b/kT} kT \tag{3}$$

Here, m, k, and h are the mass of molecule, Boltzmann's constant, and Planck's constant, respectively. We estimated that the equilibrium coverage of O_2 on CuO(111) is as small as 10^{11} cm^{-2}, or 0.05% over all Cu_{us} sites, using the parameters of our experimental conditions. Therefore, direct hopping across these "metallic" spots can only occur with rare percolation events, and the contribution of the metallic states to the change of conductance should be insignificant. Another possible mechanism for the change of conductance is the charge transfer between adsorbates and NWs. To appreciate this effect, we calculated the charge density difference (ρ_{diff}) and also performed the Bader charge analysis. Here ρ_{diff} is defined as $\rho_{diff} = \rho_{tot} - \rho_{sub} - \rho_{O_2}$, with ρ_{tot}, ρ_{sub}, and ρ_{O_2} representing the charge densities of O_2/CuO(111), clean CuO(111), and isolated O_2, respectively. As plotted in Figure 6a, O_2 molecule gains charge from the substrate, by as much as 0.19 electrons per molecule. This is expected to increase the hole density in the substrate and hence the conductance. We estimated that the change of the hole density within a depth of 10−20 Å is about 10^{18} cm^{-3}. This value is about 3−5% of the total carrier concentration (on the order of 10^{19} cm^{-3}). As a result, the conductance decreases by a few percent with the removal of O_2 molecules from CuO NWs as seen in Figure 5. Interestingly, we found that adsorption of O_2 on CuO(111) induces a sizable net magnetic moment of 2.0 μ_B, with 1.5 μ_B in the molecule and 0.5 μ_B in the substrate.

Similar effects can be found in NO_2/CuO(111). The preferential adsorption geometry of NO_2 can be found in Figure 6b. The NO_2 molecule binds to two Cu_{us} atoms, with the O−Cu_{us} bond lengths of 1.98 Å, shorter than those of O_2/CuO(111). Because NO_2 has an unpaired electron, it interacts with CuO(111) much more strongly. The binding energy is as large as 0.96 eV for NO_2/CuO(111). This leads to an equilibrium coverage of about 10^{13} cm^{-2}, about 4% over the active sites. Similar to what occurs in O_2/CuO(111), adsorption of NO_2 on CuO(111) also induces gap states around the Fermi level, as shown in Figure 7. We expect that the contribution of the

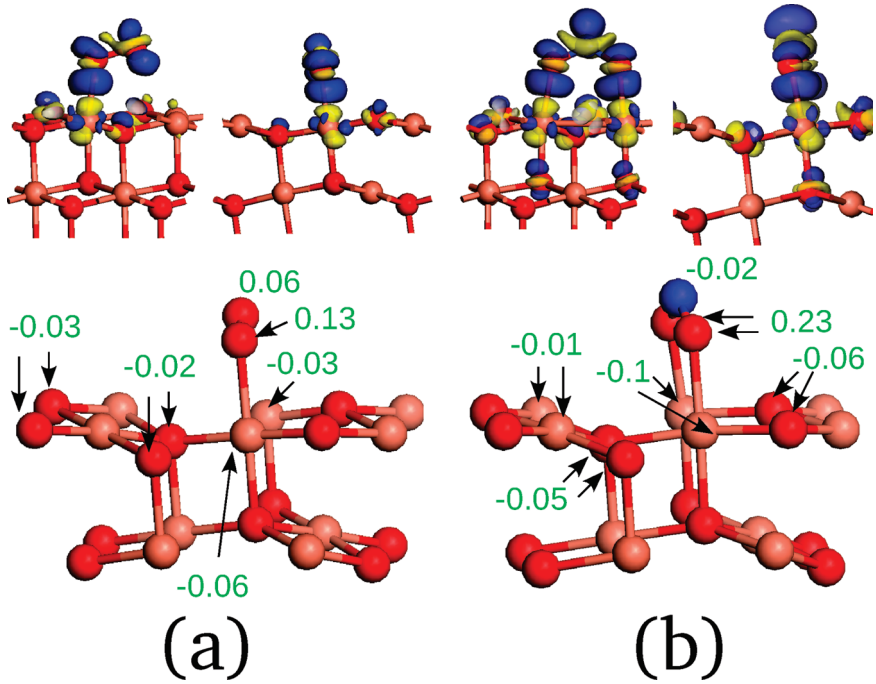

Figure 6. Isosurfaces of charge redistribution (top panel) and Bader charges (bottom panel) for (a) O_2/CuO(111) and (b) NO_2/CuO(111). The blue and yellow isosurfaces denote charge gain and depletion, respectively. Positive and negative signs of Bader charges are for gain and lose of electrons. The salmon pink, red, blue, and gray balls represent Cu, O, N, and H atoms, respectively.

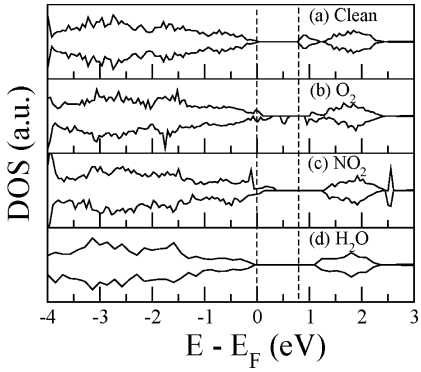

Figure 7. Density of states of (a) clean CuO(111), (b) O_2/CuO(111), (c) NO_2/CuO(111), and (d) H_2O/CuO(111). The vertical dashed lines indicate the range of band gap of the clean CuO(111) surface.

metallic feature of NO_2/CuO(111) is more significant than that of O_2/CuO(111) due to its much higher coverage. In addition, Figure 6b also clearly displays a substantial charge transfer from the substrate to NO_2. The charge gain of each NO_2 molecule is as large as 0.44 electrons, which can be converted to an increase of hole density of about $10^{19}-10^{20}$ cm^{-3}. The strong effect of NO_2 on CuO(111) is manifested in our experimental data, where the exposure of CuO NWs to 445 ppm of NO_2 gas causes 60% increase in conductance. However, it may take a longer time to achieve the fully saturated coverage, so the curve $(G - G_0)/G_0$ keeps increasing even after a few minutes in Figure 5. The net magnetic moment of NO_2/CuO(111) is 0.45 μ_B, about half that of an isolated NO_2 molecule. Furthermore, the spin polarization is very delocalized, since only 0.06 μ_B belongs to NO_2.

It is striking that C_2H_5OH molecules affect the conductance of CuO NWs oppositely at 170 and 500 °C. This is because reactions of C_2H_5OH over CuO surfaces are rather complicated, depending on the reaction temperature.[31,32] At high temperature, ethanol molecules are completely oxidized and form CO_2 and H_2O molecules as

$$C_2H_5OH + 3O_2 \rightarrow 2CO_2 + 3H_2O$$

To mimic the effect of C_2H_5OH on the conductance of CuO NWs in this regime, we investigated adsorption of CO_2 and H_2O on CuO(111). First, we found that CO_2 molecules do not bind to CuO(111), so their role in the change of conductance can be neglected. In contrast, the interaction between H_2O and CuO(111) is very strong, with an E_b of 1.24 eV. Therefore, the coverage of H_2O is high, even though the partial pressure of vapor in the environment might be small. As shown in Figure 8a, both O and H atoms interact with the substrate atoms. The $O-Cu_{us}$ bond length is 2.08 Å, and the $H-O_{us}$ bond length is 1.65 Å. The calculated DOS of H_2O/CuO(111) in Figure 7e indicates that E_g increases by about 40% compared to that of CuO(111). Furthermore, each H_2O molecule loses 0.05 electron to the substrate, opposite to what occurs in O_2/CuO(111) and NO_2/CuO(111). Both effects lead to reduction of the hole density in CuO NWs, and thus we can explain the experimental findings that the conductance of CuO NWs decreases with exposure to C_2H_5OH at 500 °C. However, it is hard to give quantitative estimation for the change in carrier density, due the large uncertainty in the partial gas pressure of H_2O in the environment.

At 170 °C, dehydrogenation of ethanol to acetaldehyde and hydrogen may occur over the surfaces of CuO NWs

$$C_2H_5OH \rightarrow CH_3CHO + H_2$$

So we expect that both CH_3CHO and C_2H_5OH may exist in the environment. Our calculations indicate that both C_2H_5OH and CH_3CHO prefer to bind with the Cu_{us} atom, as shown in parts b and c of Figure 8, with an $O-Cu_{us}$ bond length of 2.11 Å. The values of E_b for these two cases are almost the same, 0.44 and 0.42 eV, respectively. These values of E_b are consistent with previous experimental measurements.[33] However, we found that C_2H_5OH and CH_3CHO donate 0.07 and 0.03 electrons to the CuO(111) surface, respectively, as shown in parts b and c

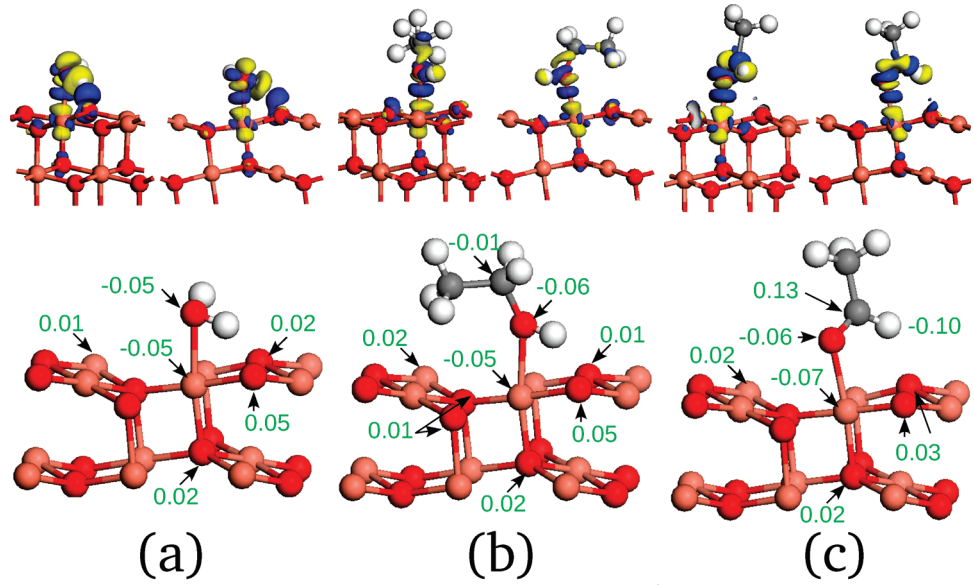

Figure 8. Isosurfaces of charge redistribution (top panel) and Bader charges (bottom panel) for (a) H_2O/CuO(111), (b) C_2H_5OH/CuO(111), and (c) CH_3CHO/CuO(111). The notations are same as in Figure 6. The dark gray balls are for C atoms.

of Figure 8. This is obviously inconsistent with our experimental observation at 170 °C, because donation of electrons to CuO(111) should decrease the hole density and hence reduce its conductance. This discrepancy likely stems from the effect that coadsorption of C_2H_5OH and CH_3CHO triggers percolation of conducting channels set by O_2 molecules on the surface. Other factors such as dissociation of C_2H_5OH on Cu vacancies and additional adsorption of O_2 facilitated by C_2H_5OH and CH_3CHO may also contribute to the increase of conductance.[25]

Another product of ethanol over CuO surface is CO.[33] We found that CO does not contribute to conductance change observed in our experiments. On one hand, CO does not interact with Cu_{us}. On the other hand, as we place a CO molecule on the top of O_{us}, CO can directly take the lattice oxygen atom away and form CO_2 via the Mars−van Krevelen mechanism. This observation is of prominent interest because the CO oxidation process does not needd to overcome any energy barrier, and the energy gain of the reaction is as high as 1.4 eV. If the substrate can reheal sufficiently fast with oxygen atoms from air, the reaction rate of CO oxidation should be very high on CuO(111) or CuO nanowires. The reaction dynamics of CO oxidization on CuO(111) deserves further study for the development of robust nanocatalysts with CuO. The creation of more oxygen vacancies should also affect transport properties of CuO NWs. Although O-vacancies are typically viewed as donors in oxide semiconductors, the electrons left behind in CuO are nevertheless localized in Cu d-orbitals and hence will not directly contribute to transport. Therefore, the actual role of oxygen vacancies on the transport and catalytic properties of CuO should be a subject of further studies.

As discussed above, CuO($\bar{1}$11) is another important facet in CuO NWs. Nevertheless, we found that it interacts with gas molecules in a very similar way as does the CuO(111) surface. For example, E_b of NO_2/CuO($\bar{1}$11) is 0.95 eV/NO_2, and 0.42 electrons transfer from the substrate to NO_2. Therefore, we do not discuss results of adsorptions on CuO($\bar{1}$11) separately.

IV. Conclusions

In summary, we investigated the stabilities, electronic structures, and surface activities of CuO surfaces, based on first-principles calculations. It was found that CuO(111) and CuO($\bar{1}$11) are the most stable surfaces and thus should be the dominant facets on CuO NWs. We found that adsorption of oxidizing gases such as O_2 or NO_2 on CuO(111) induces metallic behavior, and molecules gain electrons from the substrate. These two effects result in enhancement of conductance of CuO NWs observed in our experiments. We also studied the opposite effects of C_2H_5OH gas on the conductivity of CuO NWs in two temperature regimes. C_2H_5OH are oxidized and form CO_2 and H_2O at high temperature. While CO_2 molecules desorb, H_2O molecules tightly bind on CuO(111) and donate electrons to the substrate. This leads to reduction of conductance, as observed experimentally. The reaction of C_2H_5OH gas at low temperature on CuO NWs is less transparent, and the modification in conductivity of CuO NWs may result from coherent effects of multiple factors. We found that CuO(111) can also effectively oxidize CO through the Mars−van Krevelen mechanism.

Acknowledgment. Work in UCI was supported by DOE Grant DE-FG02-05ER46237. Work at USC was supported by NSF Grant DMR 0742225. D.L. is also grateful for the support of the China Scholarship Council and the International Scientific Collaboration Fund of Shanghai (08520705300). Calculations were performed on parallel computers at NERSC.

References and Notes

(1) Fan, Z.; Wang, D.; Chang, P. C.; Tseng, W. Y.; Lu, J. G. *Appl. Phys. Lett.* **2004**, *85*, 5923.
(2) Li, C.; Zhang, D.; Liu, X.; Han, S.; Tang, T.; Han, J.; Zhou, C. *Appl. Phys. Lett.* **2003**, *82*, 1613.
(3) Kim, I.; Rothschild, A.; Lee, B. H.; Kim, D. Y.; Jo, S. M.; Tuller, H. L. *Nano Lett.* **2006**, *6*, 2009.
(4) Liao, L.; Lu, H. B.; Li, J. C.; Liu, C.; Fu, D. J.; Liu, Y. L. *Appl. Phys. Lett.* **2007**, *91*, 173110.
(5) Ray, S. C. *Sol. Energy Mater. Sol. Cells* **2001**, *68*, 307.
(6) Hardee, K. L.; Bard, A. J. *J. Electronchem. Soc.* **1977**, *124*, 215.
(7) Koffyberg, F. P.; Benko, F. A. *J. Appl. Phys.* **1982**, *53*, 1173.
(8) Marabelli, F.; Parravicini, G. B.; Salghetti-Drioli, F. *Phys. Rev. B* **1995**, *52*, 1433.
(9) Nakamura, Y.; Yoshioka, H.; Miyayama, M.; Yanagida, H.; Tsurutani, T.; Nakamura, Y. *J. Electrochem. Soc.* **1990**, *137*, 940.
(10) Reitz, J. B.; Solomon, E. I. *J. Am. Chem. Soc.* **1998**, *120*, 11467.
(11) Wang, C.; Fu, X. Q.; Xue, X. Y.; Wang, Y. G.; Wang, T. H. *Nanotechnology* **2007**, *18*, 145506.
(12) Chen, J.; Wang, K.; Hartman, L.; Zhou, W. *J. Phys. Chem. C* **2008**, *112*, 16017.

(13) Liao, L.; Zhang, Z.; Yan, B.; Zheng, Z.; Bao, Q. L.; Wu, T.; Li, C. M.; Shen, Z. X.; Zhang, J. X.; Gong, H.; Li, J. C.; Yu, T. *Nanotechnology* **2009**, *20*, 085203.

(14) Hansen, B. J.; Kouklin, N.; Lu, G.; Lin, I. K.; Chen, J.; Zhang, X. *J. Phys. Chem. C* **2010**, *114*, 2440.

(15) Kolmakov, A.; Moskovits, M. *Annu. Rev. Mater. Res.* **2004**, *34*, 151.

(16) Norman, M. R.; Freeman, A. J. *Phys. Rev. B* **1986**, *33*, 8896.

(17) Vila, M.; Díaz-Guerra, C.; Piqueras, J. *J. Phys. D: Appl. Phys.* **2010**, *43*, 135403.

(18) Li, D. D.; Hu, J.; Chang, P. C.; Wu, R. Q.; Lu, J. G. Conductometric sensor based on Individual CuO Nanowires. (In preparation).

(19) Kresse, G.; Furthmuller, J. *Comput. Mater. Sci.* **1996**, *6*, 15. Kresse, G.; Furthmuller, J. *Phys. Rev. B* **1996**, *54*, 11169.

(20) Perdew, J. P. In *Electronic Structure of Solids*; Ziesche, P., Eschrig, H., Eds.; Akademie Verlag: Berlin, 1991.

(21) Blochl, P. E. *Phys. Rev. B* **1994**, *50*, 17953. Kresse, G.; Joubert, D. *Phys. Rev. B* **1999**, *59*, 1758.

(22) Monkhorst, H. J.; Pack, J. D. *Phys. Rev. B* **1976**, *13*, 5188.

(23) Anisimov, V. I.; Zaanen, J.; Anisimov, O. K. *Phys. Rev. B* **1991**, *44*, 943.

(24) Anisimov, V. I.; Aryasetiawan, F.; Liechtenstein, A. I. *J. Phys.: Condens. Matter* **1997**, *9*, 767.

(25) Wu, D.; Zhang, Q.; Tao, M. *Phys. Rev. B* **2006**, *73*, 235206.

(26) Dudarev, S. L.; Botton, G. A.; Savrasov, S. Y.; Humphreys, C. J.; Sutton, A. P. *Phys. Rev. B* **1998**, *57*, 1505.

(27) Forsyth, J. B.; Brown, P. J.; Wanklyn, B. M. *J. Phys. C: Solid State Phys.* **1988**, *21*, 2917.

(28) Yang, B. X.; Thurston, T. R.; Tranquada, J. M.; Shirane, G. *Phys. Rev. B* **1989**, *39*, 4343.

(29) Reuter, K.; Scheffler, M. *Phys. Rev. B* **2001**, *65*, 035406.

(30) Finocchi, F.; Barbier, A.; Jupille, J.; Noguera, C. *Phys. Rev. Lett.* **2004**, *92*, 136101.

(31) Nishiguchi, T.; Matsumoto, T.; Kanai, H.; Utani, K.; Matsumura, Y.; Shen, W. J.; Imamura, S. *Appl. Catal., A* **2005**, *279*, 273.

(32) Vaidya, P. D.; Rodrigures, A. E. *Chem. Eng. J.* **2006**, *117*, 39.

(33) Cordi, E. M.; O'Neill, P. J.; Falconer, J. L. *Appl. Catal., B* **1997**, *14*, 23.

JP1039089